

Article

{Gd^{III}₇} and {Gd^{III}₁₄} Cluster Formation Based on a Rhodamine 6G Ligand with a Magnetocaloric Effect

Lin Miao ¹, Cai-Ming Liu ² and Hui-Zhong Kou ^{1,*}

¹ Engineering Research Center of Advanced Rare Earth Materials (Ministry of Education), Department of Chemistry, Tsinghua University, Beijing 100084, China

² Beijing National Laboratory for Molecular Sciences, Center for Molecular Science, Institute of Chemistry, Chinese Academy of Sciences, Beijing 100190, China; cmliu@iccas.ac.cn

* Correspondence: kouhz@mail.tsinghua.edu.cn

Abstract: Heptanuclear {Gd^{III}₇} (complex 1) and tetradecanuclear {Gd^{III}₁₄} (complex 2) were synthesized using the rhodamine 6G ligand HL (rhodamine 6G salicylaldehyde hydrazone) and characterized. Complex 1 has a rare disc-shaped structure, where the central Gd ion is connected to the six peripheral Gd^{III} ions via CH₃O⁻/μ₃-OH⁻ bridges. Complex 2 has an unexpected three-layer double sandwich structure with a rare μ₆-O²⁻ ion in the center of the cluster. Magnetic studies revealed that complex 1 exhibits a magnetic entropy change of 17.4 J kg⁻¹ K⁻¹ at 3 K and 5 T. On the other hand, complex 2 shows a higher magnetic entropy change of 22.3 J kg⁻¹ K⁻¹ at 2 K and 5 T.

Keywords: lanthanide oxygen cluster; magnetocaloric effect; magnetic refrigerant materials; rhodamine ligand

1. Introduction

The exploration of new compounds in the field of coordination chemistry reveals many fascinating structures and properties. Among them, rare earth ions play an important role in the assembly of polynuclear clusters [1–3]. Due to their large ion radius and inherent ability to participate in various coordination environments, rare earth ions can promote the formation of polymetallic clusters [4–22]. Multinuclear rare earth clusters with different structural types, such as {Ln₁₈} [23], {Ln₂₈} [24], {Ln₃₄} [25], {Ln₃₆} [26], {Ln₃₇} [27], {Ln₄₈} [28], {Ln₆₀} [29], {Ln₇₂} [30], {Ln₁₀₄} [31], {Ln₁₄₀} [32], etc., were synthesized, and the largest even has a {Nd₂₈₈} structure [33]. These polynuclear clusters usually exhibit fascinating properties, such as single-molecule magnetism [8,12,14,15,19,30], luminescence [23,24], magneto-optical properties [34] and proton-conductive properties [35].

The formation of lanthanide hydroxide clusters involves the hydrolysis of lanthanide ions in the presence of ligands. The hydrolysis process leads to the formation of small lanthanide hydroxide units, which then assemble to form larger clusters. The size and structure of the clusters can be controlled by adjusting the hydrolysis conditions and the choice of ligands. The hydrolysis-induced assembly mechanism of lanthanide hydroxide clusters is still not fully understood due to the elusive coordination configurations of lanthanide ions and the limited characterization methods available. However, recent studies have made progress in determining the intermediate species and the pathways of cluster formation [22]. The formation of high-nuclearity lanthanide clusters is believed to involve the assembly of low-nuclearity subunits, which are formed according to initial hydrolysis. These small units are then connected to form the final cluster structure. Understanding the formation mechanism of lanthanide hydroxide clusters is important for the development of new functional materials and their applications in various fields. In addition, the interactions between the rare earth centers can affect the physical properties of the clusters. The ligand framework around these ions also plays an important role in determining the geometry, stability and functionality of the obtained clusters. By adjusting the ligand,



Citation: Miao, L.; Liu, C.-M.; Kou, H.-Z. {Gd^{III}₇} and {Gd^{III}₁₄} Cluster Formation Based on a Rhodamine 6G Ligand with a Magnetocaloric Effect. *Molecules* **2024**, *29*, 389. <https://doi.org/10.3390/molecules29020389>

Academic Editors: Andrea Bencini and Vito Lippolis

Received: 30 December 2023

Revised: 9 January 2024

Accepted: 10 January 2024

Published: 12 January 2024



Copyright: © 2024 by the authors. Licensee MDPI, Basel, Switzerland. This article is an open access article distributed under the terms and conditions of the Creative Commons Attribution (CC BY) license (<https://creativecommons.org/licenses/by/4.0/>).

scientists can strategically guide the self-assembly process, thus generating the required multi-core architecture.

Certain gadolinium compounds have shown excellent magnetocaloric properties [36–38], such as $\text{Gd}(\text{HCOO})_3$ [39], $\text{Gd}(\text{OH})_3$ [40], $\text{Gd}_2\text{O}(\text{OH})_4(\text{H}_2\text{O})_2$ [40], GdPO_4 [41], $\text{Gd}(\text{OH})\text{CO}_3$ [42], GdF_3 [43], $\text{Gd}(\text{OH})\text{F}_2$ [44] and $\text{Ba}_2\text{Gd}(\text{BO}_3)_2\text{X}$ ($\text{X} = \text{F}, \text{Cl}$) [45]. The magnetocaloric effect (MCE) in Gd is particularly strong, making it an ideal material for use in extremely low-temperature magnetic refrigeration systems. Magnetic refrigeration is a technology that uses a magnetic field to cool objects. Magnetic refrigeration materials play an increasingly important role in the future of social development, particularly in the area of energy efficiency and sustainability. In addition, molecular clusters with diverse structures also exhibit enormous magnetic cooling potential and exhibit many physical properties, such as chirality, spin crossover, fluorescence, etc.

Rhodamine-derived ligands show ring-opened or ring-closed structures and can form rare earth [46–49] or transition metal [50,51] complexes. They are mostly mononuclear or low-nuclearity complexes. We are interested in forming high-nuclearity clusters based on rhodamine ligands using the hydrolysis approach. In this work, we used the rhodamine 6G salicylaldehyde hydrazone ligand (Figure 1) to synthesize two different metal complexes, hexagonal heptanuclear $\{\text{Gd}^{\text{III}}_7\} [\text{Gd}_7(\text{L})_6(\mu_2\text{-CH}_3\text{O})_4(\mu_3\text{-CH}_3\text{O})_4(\mu_3\text{-OH})_4(\text{NO}_3)_2]\text{NO}_3 \cdot 10\text{CH}_3\text{CN} \cdot 10\text{CH}_3\text{OH} \cdot 2\text{H}_2\text{O}$ (complex 1) and tetradecanuclear $\{\text{Gd}^{\text{III}}_{14}\} \text{Gd}_{14}(\text{H}_{0.5}\text{L})_8(\mu_6\text{-O})(\mu_4\text{-O})_2(\mu_3\text{-OH})_{16}(\text{NO}_3)_{16} \cdot 9.5\text{CH}_3\text{CN} \cdot 2\text{CH}_3\text{OH} \cdot 11\text{H}_2\text{O}$ (complex 2), with an unexpected three-layer double sandwich structure. These two complexes have an excellent magnetic refrigeration performance, and their magnetic entropy changes are $17.4 \text{ J kg}^{-1} \text{ K}^{-1}$ at 3 K and 5 T and $22.3 \text{ J kg}^{-1} \text{ K}^{-1}$ at 2 K and 5 T, respectively.

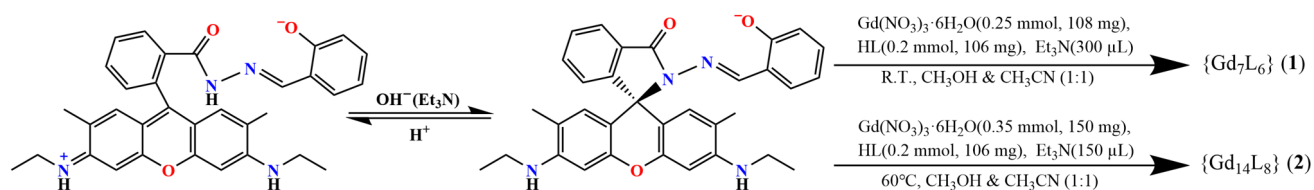


Figure 1. Transformation of ring-opened and ring-closed form of rhodamine-6G-type ligands and their reactions.

2. Results and Discussion

2.1. Synthesis and Characterization

Rhodamine 6G-type ligands have attracted significant attention in the realm of fluorescent sensors. Previous studies have primarily focused on the synthesis of mononuclear rare earth or transition metal complexes [46–52]. However, these ligands have yet to be fully unearthed. We speculate that the reaction between Ln^{III} and the rhodamine 6G ligands might lead to high-nuclearity lanthanide complexes under high pH values. Using the hydrolysis strategy, we have successfully synthesized two new Gd^{III} clusters, **1** and **2** (Figure 1). Additionally, our research has unveiled the influential factors that impact the synthesis process, including the ratio of central ions to ligands, solvents, alkalines and reaction temperature.

The synthetic procedure for the two clusters is similar, with the exception of the molar ratio of $\text{Gd}:\text{L}$, i.e., an excess amount of gadolinium nitrate was used in the synthesis of $\{\text{Gd}_{14}\}$. Both complexes were prepared using the reaction of the ligand HL with gadolinium nitrate in a mixed solution of methanol and acetonitrile. A quantity of triethylamine was used to induce the ring closure of the HL and hydrolysis, which was characterized using the UV-Vis spectra of the reactant mixtures (Figure 2). The absorption at 535 nm due to the ring-opened xanthene disappeared after the addition of four times the amount of Et_3N , revealing that the HL ligands were ring-closed [46–48]. The peak at 400 nm is most likely due to the conjugated salicylaldehyde hydrazone group, corresponding to the yellow color of the final products. The resulting mixture was left undisturbed at room temperature for one

week, facilitating the formation of yellow plate-like single crystals for $\{Gd_7\}$. The reactant mixture was heated at 60 °C in an oven for three days, resulting in the formation of yellow cubic-shaped samples of $\{Gd_{14}\}$. These two complexes tend to lose solvents in the air. When the crystals are taken out of the solution, they turn from yellow to red at room temperature, and they lose their crystallinity. The powder XRD pattern for Gd_7 illustrates that the main strong peaks show disagreement with those simulated, indicating the desolvation of the crystals (Figure S1). Thermogravimetric analysis (TGA) shows that the crystals lose all their crystallization solvent molecules to give a desolvated solid (Figure S2). The peaks at low 2θ angles in the PXRD data for Gd_{14} are approximately consistent with those simulated, and the TGA data show a weight loss of 8.5% in the temperature range 41–112 °C, which is in agreement with the calculated data of 7.7%. The infrared spectra of complexes 1 and 2 (Figure S3) show peaks at 1363 cm^{-1} and 1380 cm^{-1} , respectively, as is characteristic of nitrate anions. The disappearance of the peak at 1680 cm^{-1} for HL illustrates the coordination of aryl oxygen toward Gd^{III} . The strong peak at 1620 cm^{-1} is most likely due to the C=N stretching vibration for the Schiff base ligand L^- . The UV-Vis and fluorescent spectra (Figure 2) for the reactant solutions of HL and $Gd(NO_3)_3$ with different amounts of Et_3N were measured in the methanolic solution ($[HL] = [Gd^{3+}] = 10\text{ }\mu\text{M}$, $\lambda_{ex} = 354\text{ nm}$). The colorless ligand shows no absorption in the visible region; however, after the addition of Gd^{III} , the ligand becomes ring-opened owing to the coordination and has a strong typical absorption at 533 nm. With the addition of Et_3N , the absorption gradually decreases owing to the ring-closure of HL in alkaline conditions. The free ligand HL in MeOH has an emission at 555 nm, which is due to the presence of small quantities of the ring-opened ligand. After the addition of Gd^{III} , the ligand HL becomes ring-opened, and emits yellow light with a wavelength of 580 nm. When three times the amount of Et_3N was added, the emission nearly disappeared, indicating that almost all the HL ligands were in the ring-closed form. The complexes are slightly soluble in MeOH, and the solutions (10 μM) show an intense absorption at 398 nm, corresponding to the yellow color of the complex with ring-closed L^- ligands (Figure S4a). The emissions at 546 nm for Gd_7 and 550 nm for Gd_{14} ($\lambda_{ex} = 354\text{ nm}$) potentially come from the ring-opened xanthene in the complexes, and although the ring-opened dissociation is scant, the emission is strong. The weak emission at 484 for Gd_7 and 489 nm for Gd_{14} is most likely due to the Schiff base part of the ligand L^- (Figure S4b).

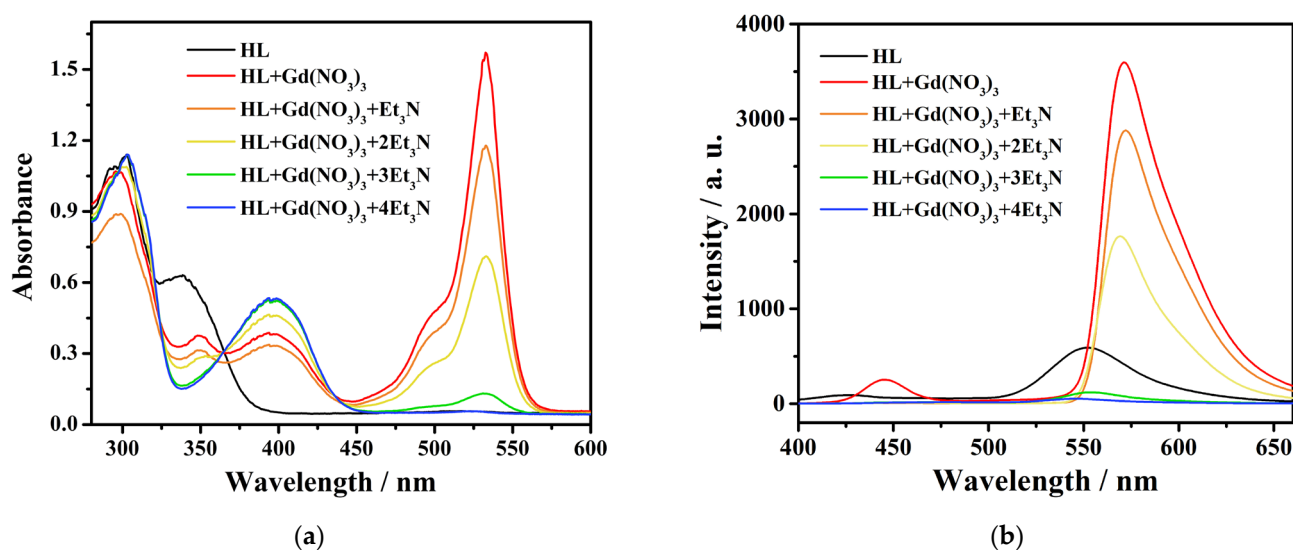


Figure 2. UV-Vis (a) and fluorescent spectra ($\lambda_{ex} = 354\text{ nm}$) (b) for the ligand HL and the reaction mixture containing HL and $Gd(NO_3)_3$ with different amounts of Et_3N in MeOH.

2.2. Structure

A yellow single crystal of complex **1** was selected for single crystal X-ray diffraction at 100 K. Complex **1** crystallizes in the monoclinic system with the $P2_1/n$ space group. The volume of the unit cell is very large with a monoclinic system, and therefore the diffraction data are not optimal. The command MASK was used during the structural refinement, and 452 electrons were masked per formula unit, which account for the missing NO_3^- anion and 10 acetonitrile, 10 methanol and 2 H_2O molecules, with their total electrons being 451. The crystallographic data and selected bond distances and angles are given in Tables S1 and S2. The asymmetric unit cell contains three crystallographically independent $\{\text{Gd}^{\text{III}}_7\}$ moieties. Because they have similar molecular structures, only one of them is described in detail as a representative. The coordination number of each Gd^{III} ion in $\{\text{Gd}_7\}$ (Figure 3) is between 7 and 9. Their coordination patterns are shown in Figures S5 and S6. Using the SHAPE software (version 2.1) for calculation, their coordination patterns were obtained, as shown in Tables S3–S5. The central Gd^{III} ions are coordinated by eight oxygen atoms and have a square antiprism structure D_{4d} . Among the eight oxygen atoms, four are $\mu_3\text{-OH}^-$ and another four are $\mu_3\text{-CH}_3\text{O}^-$. The $\text{Gd}\text{-O}_{\text{hydroxy}}$ bond distances are in the range of 2.316(9)–2.358(9) Å, slightly shorter than that of the $\text{Gd}\text{-O}_{\text{methoxy}}$ bonds (2.362(9)–2.404(6) Å). The remaining six Gd^{III} ions are evenly distributed around the central Gd^{III} ion, forming a saddle-shaped structure, which is relatively rare in rare earth complexes [53] (Figure S7). Each peripheral Gd^{III} ion is chelated by one ring-closed ligand L^- , and is bridged to the adjacent peripheral Gd^{III} ions by $\mu_2\text{-CH}_3\text{O}^-$ or phenoxy oxygen atoms (Figure 4). The $\text{Gd}\text{-O}_{\text{methoxy}}$ bond distances are in the range of 2.261(10)–2.298(10) Å, comparable to that of the $\text{Gd}\text{-O}_{\text{phenoxy}}$ bonds (2.189(10)–2.433(9) Å). The central Gd^{III} ion is connected to the six peripheral Gd^{III} ions via the $\mu_3\text{-OH}^-$ and $\mu_3\text{-CH}_3\text{O}^-$ bridges, giving rise to a Gd_7 core, as shown in Figure 3b. The bridging $\text{Gd}\text{-O}\text{-Gd}$ bond angles are in the range of 92.9(3)–110.6(4)° for $\mu_3\text{-OH}^-$, 92.9(3)–99.2(3)° for $\mu_3\text{-CH}_3\text{O}^-$, 110.4(4)–112.8(4)° for $\mu_2\text{-CH}_3\text{O}^-$ and 98.2(3)–98.4(3)° for $\mu_2\text{-O}_{\text{phenoxy}}$, respectively, with intramolecular $\text{Gd}\text{-Gd}$ separations of 3.5064(11)–3.808(11) Å. The neighboring Gd_7 molecules are connected via weak intermolecular forces and no obvious intermolecular hydrogen bonds are found based on the squeezed model of the crystal data.

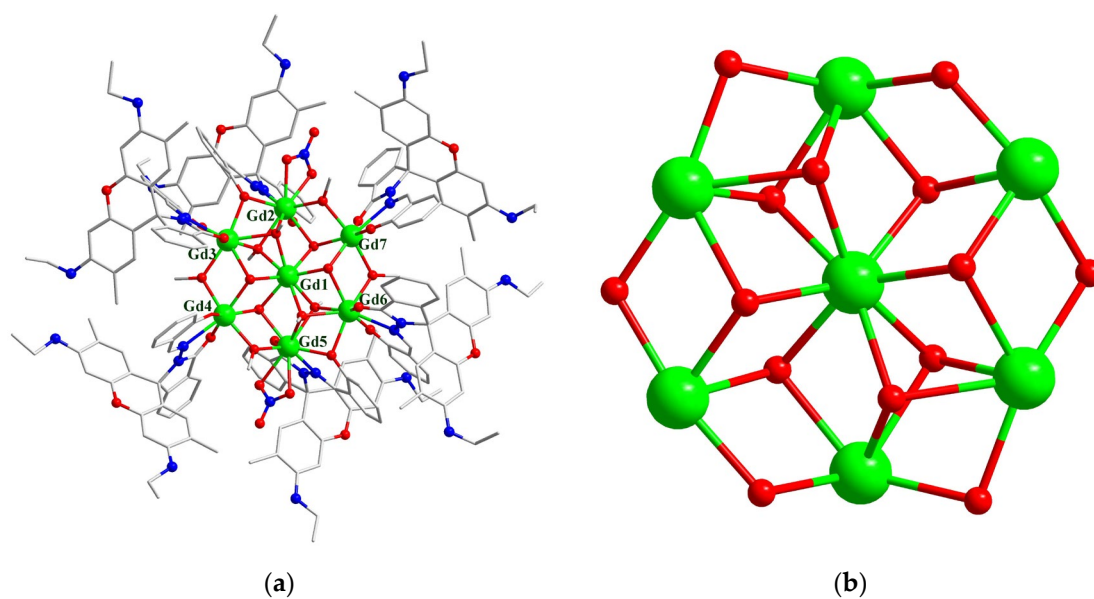


Figure 3. (a) The structure of the $\{\text{Gd}^{\text{III}}_7\}$ cation for complex **1**. Hydrogen atoms and solvents have been omitted for clarity. (b) The core skeleton graph of complex **1**. Color code: Gd^{III} green; O red; N blue; C gray.

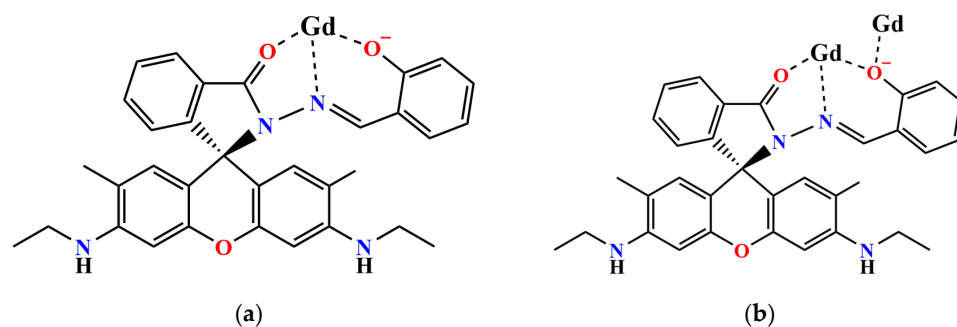


Figure 4. Schematic diagram of two different coordination modes of ring-closed rhodamine ligands L^- . (a) Tridentate chelating mode; (b) phenolic oxygen bridging mode.

As for complex **2**, a yellow cube-shaped single crystal was selected for single crystal X-ray diffraction at 173 K. A solvent mask was used, and 183.4 electrons were found at a volume of 3448.9 \AA^3 in nine voids per unit cell, which is consistent with the presence of 2 CH_3OH , 2 H_2O and 1.5 CH_3CN molecules per formula unit with 178 electrons. The crystallographic data and selected bond distances and angles are given in Tables S1 and S6. Complex **2** crystallizes in the tetragonal system with a space group of $P4/n$ and has a D_{4h} symmetry. The asymmetric unit contains 1/4 of the tetradecanuclear molecule and there are five different kinds of nine-coordinated Gd^{III} ions (Gd1-Gd5 , Figure 5b). They have three different coordination modes (Table S7) and their coordination patterns are shown in Figures S8 and S9. The tetradecanuclear cluster core is neutral and has a highly symmetrical three-layer double sandwich structure (Figure 5b). In the structure, four nine-coordinated Gd^{III} ions form a square plane layer, and a nine-coordinated Gd^{III} ion is located between the layers. The distance between the two layers is 5.792 \AA . The center of the middle layer is six-coordinated $\mu_6\text{-O}^{2-}$, while the outer layers on both sides are $\mu_4\text{-O}^{2-}$. The sandwiched Gd^{III} ions and the square-shaped layer are connected by $\mu_3\text{-OH}^-$ ions. The Gd ions are linked together by hydroxo bridges, forming a $[\text{Gd}_{14}(\mu_6\text{-O})(\mu_4\text{-O})_2(\mu_3\text{-OH})_{16}]$ core. This core contains one octahedral $[\text{Gd}_6(\mu_6\text{-O})(\mu_3\text{-OH})_8]$ unit that shares two apexes with two $[\text{Gd}_5(\mu_4\text{-O})(\mu_3\text{-OH})_4]$ square pyramid moieties. The cluster core is surrounded by eight ring-closed L^- ligands. Additionally, the Gd^{III} of the middle layer is coordinated with two nitrate ions, and the Gd^{III} of outer layers on both sides is coordinated with a nitrate ion and a tridentate ring-closed L^- ligand. The square plane layers are bridged by phenolic oxygen on the ligand, as shown in Figure 4b. Unlike in complex **1**, all the ligands L^- are involved in the bridging, and none of the coordination modes shown in Figure 4a are present in complex **2**.

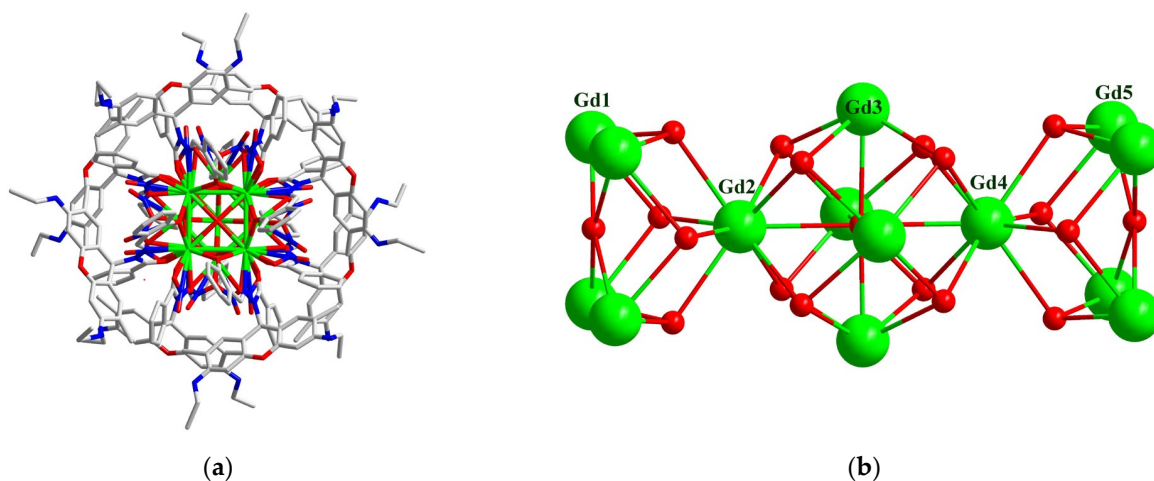


Figure 5. (a) The structure of complex **2**. Hydrogen atoms and solvents have been omitted for clarity. (b) The core skeleton of complex **2**. Color code: Gd^{III} green; O red; N blue; C gray.

As for the coordination environment of the Gd₁₄ ions, three different types can be divided into Gd1 and Gd5 and their equivalences; Gd2 and Gd4; Gd3 and its equivalences. The Gd1 or Gd5 ion is surrounded by two μ_3 -OH⁻, two μ_2 -phenoxy, one μ_4 -O²⁻ and one L⁻ ligand, with Gd–O/N bond distances of 2.320(7)–2.587(19) Å for Gd1 and 2.292(8)–2.601(11) Å for Gd5. The Gd2 or Gd4 ion is coordinated by eight μ_3 -OH⁻ and one μ_6 -O²⁻, with Gd–O bond distances of 2.434(9)–2.617(13) Å for Gd2 and 2.454(8)–2.716(13) Å for Gd4. The Gd3 ion is coordinated by one μ_6 -O²⁻, four μ_3 -OH⁻ and two nitrate anions, with Gd–O bond distances of 2.335(8)–2.555(9) Å. The rare μ_6 -O²⁻-bridged Gd₆ core has an elongated octahedral symmetry, with equatorial Gd–O bond distances of 2.4822(8) Å and axial Gd–O bond distances of 2.617(13)/2.716(13) Å. The intermetallic Gd–Gd separations within the Gd₁₄ core are similar and are in the range of 3.5099(11)–3.882(1) Å. The Gd–O–Gd bond angles via the μ_3 -OH⁻ bridges are in the range of 95.9(3)–107.8(4)°, and those via the phenoxy bridges are similar (97.5(3) and 97.8(3)°). The acetonitrile molecules are hydrogen-bonded to the HN groups of L⁻. No intermolecular π – π contact is observed. The nearest intermolecular Gd–Gd separation is 13.73 Å.

Although there are many reports on tetranuclear clusters of planar quadrilateral [54,55] and nona-nuclear molecules of the double-layer sandwich type [56,57], a rare earth molecular structure in the form of a three-layer double sandwich is uncommon. Similar molecules have been reported before, as shown in Figures S10–S12. Tetradecanuclear hydroxo-lanthanide acetylacetonato complexes, formulated as Ln₁₄(μ_4 -OH)₂(μ_3 -OH)₁₆(μ - η^2 -acac)₈(η^2 -acac)₁₆ (Ln = Tb and Eu, acac⁻ = acetylacetonato) [58], and chiral tetradecanuclear hydroxo-lanthanide clusters, as Ln₁₄(μ_4 -OH)₂(μ_3 -OH)₁₆(μ - η^2 -acac)₈(η^2 -acac)₁₆·6H₂O (Ln = Dy and Tb) [59], have been reported. The ligands used in these two works are both based on acetylacetonato, but the present tetradecanuclear {Gd^{III}₁₄} is a completely different ligand, i.e., ring-closed rhodamine L⁻. The use of ortho-nitrophenolate exhibited the tetradecanuclear H₁₈[Ln₁₄(μ - η^2 -o-O₂N-C₆H₄O)₈(η^2 -o-O₂N-C₆H₄O)₁₆(μ_4 -O)₂(μ_3 -O)₁₆] (Ln = Dy and Tm; o-O₂N-C₆H₄O⁻ = o-nitrophenolate) [60]. Despite the above similar Ln₁₄ complexes, the μ_6 -O²⁻ in **2** is unique among them.

It is worth mentioning that similar hexadecanuclear molecules [Eu^{III}₁₆(tfac)₂₀(CH₃OH)₈(μ_3 -OH)₂₄(μ_6 -O)₂] have also been reported based on trifluoroacetylacetonato (tfac⁻) [22]. In addition to the tetradecanuclear {Eu₁₄} core, there are another two Eu ions on the opposite sides (Figure S13). This study provides insights into the formation, evolution and assembly of lanthanide hydroxide clusters. The formation of {Gd₇} and {Gd₁₄} in this work further verifies that hydrolysis under high pH values is an effective way of constructing high-nuclearity Ln^{III} species.

2.3. Magnetic Measurements

The temperature dependence of the magnetic susceptibility of complexes **1** and **2** is measured under a 1000 Oe magnetic field in the range of 2–300 K (Figure 6). At room temperature, the $\chi_M T$ values of 54.1 cm³ K mol⁻¹ for {Gd₇} and 109.0 cm³ K mol⁻¹ for {Gd₁₄} are close to the theoretical values of 55.09 cm³ K mol⁻¹ for heptanuclear and 110.18 cm³ K mol⁻¹ for tetradecanuclear uncoupled Gd^{III} ($S = 7/2$, $g = 2$, $C = 7.87$ cm³ K mol⁻¹ per Gd), respectively. For **1**, upon lowering the temperature, the $\chi_M T$ value slightly decreases to 49.76 cm³ K mol⁻¹ at 20 K and then rapidly falls to 30.22 cm³ K mol⁻¹ at 2 K. Complex **2** exhibits a similar behavior: when lowering the temperature, the $\chi_M T$ value slightly decreases to 95.4 cm³ K mol⁻¹ at 30 K, and then rapidly falls to 33.0 cm³ K mol⁻¹ at 2 K. These changes indicate the presence of dominant antiferromagnetic interactions between the Gd^{III} ions in the clusters. The data can be perfectly fitted to the Curie–Weiss law, giving $C = 54.44$ cm³ K mol⁻¹ and $\theta = -1.71$ K for {Gd₇} and $C = 110.50$ cm³ K mol⁻¹ and $\theta = -4.63$ K for {Gd₁₄} (Figure S14). The larger absolute θ value in {Gd₁₄} suggests that the antiferromagnetic interaction is stronger than that for {Gd₇}.

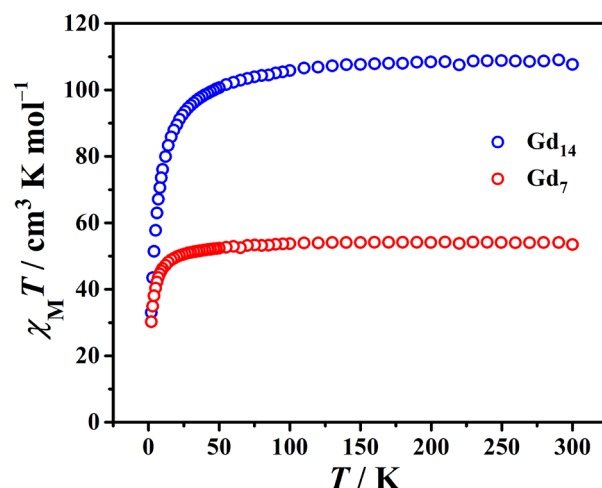


Figure 6. Temperature dependence of $\chi_M T$ for $\{\text{Gd}_7\}$ and $\{\text{Gd}_{14}\}$ under a 1000 Oe magnetic field in the range of 2–300 K.

The field dependence of the magnetizations (M) for complexes **1** and **2** was measured in the temperature range of 2–10 K (Figure S15). It can be seen that the magnetization has not reached saturation at 5 T and 2 K. At 2 K, the experimental maximum magnetization values of 47.03 $N\beta$ for **1** and 89.35 $N\beta$ for **2** are lower than the theoretical saturation value of Gd^{III} (49 $N\beta$ for **1** and 98 $N\beta$ for **2**, respectively), which may owe to the antiferromagnetic coupling, and a higher magnetic field is needed to suppress the magnetic coupling effect. For complexes **1** and **2**, the experimental M – H curves at 2–10 K lie below the calculated Brillouin curve for non-interacting S_{Gd} spins (Figures S16 and S17), also suggesting the presence of overall intermetallic antiferromagnetic coupling. The difference between the experimental and calculated values for Gd_{14} is obviously larger than that for Gd_7 , indicating that the former shows stronger antiferromagnetic coupling than that of the latter. The presence of $\mu_6\text{-O}^{2-}$ -bridged Gd_6O moiety may be responsible for this.

The half-filled 4f electronic configuration in Gd^{III} ions makes them magnetically isotropic. This makes gadolinium a valuable material in various applications, especially magnetic refrigeration. Thus, the magnetocaloric effect (MCE) of complexes **1** and **2** was studied using the Maxwell equation:

$$\Delta S_m(T)_{\Delta H} = \int \left[\frac{\partial M(T, H)}{\partial T} \right]_H dH$$

At 3 K and $\Delta H = 5$ T, the value of $-\Delta S_m$ is 17.44 $\text{J kg}^{-1} \text{K}^{-1}$ for **1** (Figure 7a), which is slightly lower than the expected value of 14.56R (25.25 $\text{J kg}^{-1} \text{K}^{-1}$) calculated for seven uncorrelated Gd^{III} ions using the equation $-\Delta S_m = nR \ln(2S + 1)$ ($R \approx 8.314 \text{ J mol}^{-1} \text{K}^{-1}$). The value of $-\Delta S_m$ for **2** is 22.30 $\text{J kg}^{-1} \text{K}^{-1}$ at 2 K and $\Delta H = 5$ T (Figure 7b), which is close to the expected value of 29.11R (28.72 $\text{J kg}^{-1} \text{K}^{-1}$) calculated for 14 uncorrelated Gd^{III} ions. To improve the magnetic refrigeration effect of the gadolinium clusters [37], several approaches can be considered. Firstly, the experimental conditions can be optimized. For instance, the temperature and magnetic field can be carefully controlled to ensure the most efficient operation of the gadolinium clusters. The thermal conductivity of the environment and the pressure during the refrigeration cycle can also be adjusted to minimize the energy loss. Secondly, the chemical composition of the clusters can be varied. Gadolinium can be alloyed with other metals to create compounds with different magnetic properties. Thirdly, the size of the clusters can be optimized. The optimal size will depend on the specific setup and application, but generally smaller clusters have a higher surface-to-volume ratio, which leads to more efficient heat exchange and therefore a stronger refrigeration effect. However, too-small clusters may also suffer from higher energy barriers between spin states, which can decrease the magnetic entropy change. Overall, a combination of these

strategies can be used to improve the magnetic refrigeration effect of gadolinium clusters for various applications, such as cryogenic cooling of scientific instruments, temperature control in electronics and energy-efficient refrigeration in households and industries.

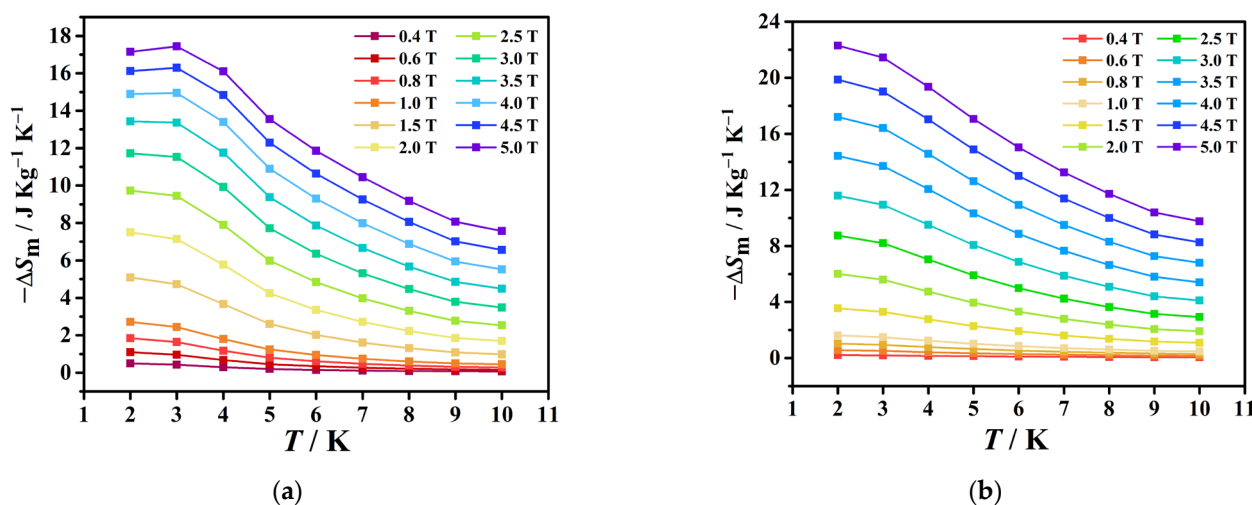


Figure 7. Experimental $-\Delta S_m$ values of 1 (a) and 2 (b) for multiple temperatures and magnetic fields calculated from magnetization data.

3. Materials and Methods

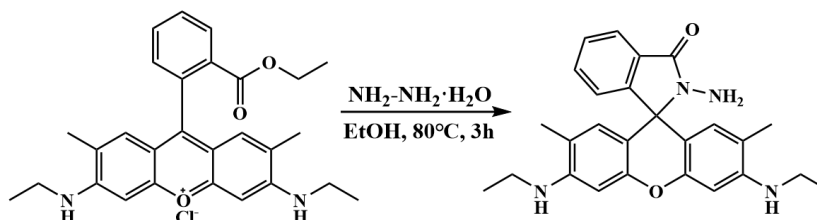
3.1. Synthesis and Preparations

All of the reagents we used were commercially available and used without further purification. The ligand HL we used was synthesized according to the method in the literature [46–49].

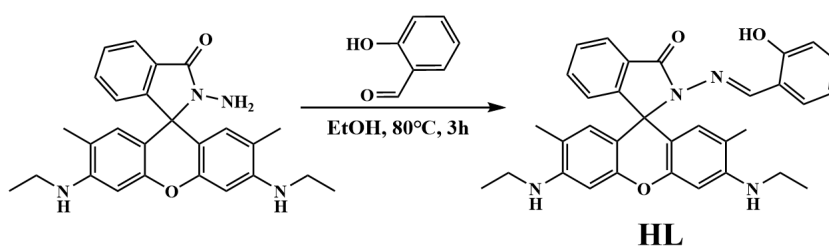
3.1.1. Synthesis of the Ligand HL

Step 1: Synthesis of Rhodamine 6G hydrazide. Solid rhodamine 6G (10 mmol, 4.5 g) was dissolved in ethanol (100 mL). During stirring, 80% hydrazine hydrate solution (10 mL) was slowly added, and then the mixture was heated at 80 °C. After refluxing for 3 h, the reaction solution was cooled to room temperature. A light-colored precipitate was generated from the orange solution, which was collected using filtration, and washed with deionized water and ethanol until the color of the product turned white. Yield: about 4 g.

Caution: As hydrazine hydrate is a highly toxic reagent, the operations should be performed in a fume hood with care.



Step 2: Synthesis of HL. Rhodamine 6G hydrazide (5 mmol, 2.22 g) was suspended in 100 mL ethanol under stirring and heating at 80 °C, to which salicylaldehyde (10 mmol, 1 mL) was slowly added. The reaction continued at 80 °C for 3 h, and then the mixture was cooled to room temperature to give a light-colored solid. Filtering and washing with deionized water and ethanol generated a white solid powder of HL (about 2 g). The solid was used without further purification.



3.1.2. Synthesis of

$[\text{Gd}_7(\text{L})_6(\mu_2\text{-CH}_3\text{O})_4(\mu_3\text{-CH}_3\text{O})_4(\mu_3\text{-OH})_4(\text{NO}_3)_2]\text{NO}_3 \cdot 10\text{CH}_3\text{CN} \cdot 10\text{CH}_3\text{OH} \cdot 2\text{H}_2\text{O}$ (1)

The ligand HL (0.2 mmol, 106 mg) was suspended in a mixed solution of MeOH (10 mL) and MeCN (10 mL), to which $\text{Gd}(\text{NO}_3)_3 \cdot 6\text{H}_2\text{O}$ (0.25 mmol, 108 mg) was added, generating a red solution. The solution was heated and stirred for a few minutes and then triethylamine (300 μL , 2.16 mmol) was added to give a yellow solution. The mixture was filtered and the filtrate was placed undisturbed at room temperature. Yellow crystals suitable for X-ray diffraction analysis were collected after about 7 days. Yield: about 20%. Desolvated samples were used for the elemental analysis and physical measurements. Elemental analysis calcd. (%) for $\text{C}_{206}\text{H}_{214}\text{N}_{27}\text{O}_{39}\text{Gd}_7$ (4793.23): C, 51.62; H, 4.50; N, 7.89. Found: C, 51.79; H, 4.91; N, 7.92.

3.1.3. Synthesis of

$\text{Gd}_{14}(\text{H}_{0.5}\text{L})_8(\mu_6\text{-O})(\mu_4\text{-O})_2(\mu_3\text{-OH})_{16}(\text{NO}_3)_{16} \cdot 9.5\text{CH}_3\text{CN} \cdot 2\text{CH}_3\text{OH} \cdot 11\text{H}_2\text{O}$ (2)

The ligand HL (0.2 mmol, 106 mg) was suspended in the mixed solution of MeOH (10 mL) and MeCN (10 mL). $\text{Gd}(\text{NO}_3)_3 \cdot 6\text{H}_2\text{O}$ (0.35 mmol, 150 mg) was added to generate a red solution. After heating and stirring for a few minutes, triethylamine (150 μL , 1.08 mmol) was added, giving rise to a yellow solution. The solution was filtered and the filtrate was heated in an oven at 60 °C. Yellow crystals suitable for X-ray diffraction analysis were obtained after about 2 days and collected. Yield: about 30%. Elemental analysis calcd. (%) for $\text{C}_{285}\text{H}_{330.5}\text{N}_{57.5}\text{O}_{104}\text{Gd}_{14}$ (8427.05): C, 39.62; H, 3.95; N, 9.56. Found: C, 39.27; H, 4.10; N, 9.25.

3.2. Physical Measurements

The elemental analyses (C, H and N) were performed using an Elementar Vario Carlo Erballo analyzer. The powder X-ray diffraction (PXRD) measurements were recorded on a Bruker D8 ADVANCE X-ray diffractometer using $\text{CuK}\alpha$ radiation ($\lambda = 1.54184 \text{ \AA}$) at room temperature from 5° to 50° with a sweeping speed of 10°/min. The single-crystal X-ray data were collected using a Rigaku SuperNova, Dual, Cu at zero, AtlasS2. The structure was solved using the program Olex2 1.3 and refined using a full-matrix least-squares method based on F^2 using the SHELXL-2018/3 method. Hydrogen atoms were added geometrically and refined using a riding model. The temperature- and field-dependent magnetic susceptibility measurements were carried out using a Quantum Design MPMS XL5 SQUID magnetometer. The IR spectra (KBr tablet) were recorded on the WQF 510A FTIR equipment in the range of 400–4000 cm^{-1} with a sweeping interval of 2 cm^{-1} . The UV-Vis absorption spectra were measured using a TU-1901 spectrophotometer in the range of 280–600 nm with a sweeping interval of 0.5 nm. The photoluminescence spectra were measured using a Lengguang F98 fluorescence spectrophotometer. The sweeping speed was 1000 nm/min with a sweeping interval of 1 nm.

4. Conclusions

In conclusion, novel high-nuclearity clusters have been obtained using the hydrolysis strategy: saddle-shaped $\{\text{Gd}_7\}$ and a three-layer double sandwich $\{\text{Gd}_{14}\}$. Both complexes exhibit good magnetocaloric properties with magnetic entropy changes of 17.4 $\text{J kg}^{-1} \text{ K}^{-1}$ for Gd_7 at 3 K and 5 T and 22.3 $\text{J kg}^{-1} \text{ K}^{-1}$ for Gd_{14} at 2 K and 5 T, respectively. Further work on the new clusters $\{\text{Ln}^{\text{III}}_7\}$ and $\{\text{Ln}^{\text{III}}_{14}\}$ (Ln = Dy, Tb, Eu and Ho) are in progress in our laboratory, which possibly behave as SMMs or fluorescent materials. The combination

of rare earth ions and new ligands paves the way for the discovery of new polynuclear clusters with unprecedented structures and functionalities.

Supplementary Materials: The following supporting information can be downloaded at <https://www.mdpi.com/article/10.3390/molecules29020389/s1>. Table S1. Crystal data and refinement parameters for complexes **1** and **2**; Table S2. Selected bond distances (Å) and bond angles (°) for complex **1**; Table S3. The results of coordination geometric configurations evaluated by SHAPE software for seven-coordinated Gd of complex **1**; Table S4. The results of coordination geometric configurations evaluated by SHAPE software for eight-coordinated Gd of complex **1**; Table S5. The results of coordination geometric configurations evaluated by SHAPE software for nine-coordinated Gd of complex **1**; Table S6. Selected bond distances (Å) and bond angles (°) for complex **2**; Table S7. The results of coordination geometric configurations evaluated by SHAPE software for nine-coordinated Gd of complex **2**; Figure S1. Powder diffraction pattern of complexes **1** and **2**; Figure S2. Thermogravimetric analysis of complexes **1** and **2**; Figure S3. IR spectra of HL, complexes **1** and **2**; Figure S4. UV-vis (a) and fluorescence spectra ($\lambda_{\text{ex}} = 354 \text{ nm}$, b) for complexes Gd₇ (**1**) and Gd₁₄ (**2**) in MeOH (10 μM); Figure S5. Top and side view of the heptanuclear surrounding polyhedral structures for complex **1**; Figure S6. The coordinate lanthanide Gd^{III} surrounding polyhedral structures for complex **1**; Figure S7. Structure of [Gd₇(OH)₆(thmeH₂)₅(thmeH)(tpa)₆(MeCN)₂]²⁺ (Gd (purple), O (yellow), N (blue), C (skeletal), H atoms are not shown); Figure S8. Drawings of the tetradecanuclear surrounding polyhedral structures for complex **2**; Figure S9. Drawings of the coordinate lanthanide Gd^{III} surrounding polyhedral structures for complex **2**; Figure S10. The molecular structure of Ln₁₄(μ_4 -OH)₂(μ_3 -OH)₁₆(μ - η^2 -acac)₈(η^2 -acac)₁₆ (Ln = Tb and Eu, acac[−] = acetylacetonato); Figure S11. Polyhedral representation of the structure of Ln₁₄(μ_4 -OH)₂(μ_3 -OH)₁₆(μ - η^2 -acac)₈(η^2 -acac)₁₆·6H₂O (Ln = Dy and Tb) cluster core; Figure S12. Solid-state structure of H₁₈[Ln₁₄(μ - η^2 -o-O₂N-C₆H₄-O)₈(η^2 -o-O₂N-C₆H₄-O)₁₆(μ_4 -O)₂(μ_3 -O)₁₆] (Ln = Dy, Er, Tm, Yb; o-O₂N-C₆H₄-O = o-nitrophenolate) showing the atom labeling scheme, omitting hydrogen atoms; Figure S13. Polyhedron view of the [Eu₁₆(tfac)₂₀(CH₃OH)₈(μ_3 -OH)₂₄(μ_6 -O)₂] cluster where ligands have been removed for clarity; Figure S14. Temperature dependence of χ_{MT} for **1** (up) and **2** (bottom) under a 1000-Oe magnetic field in the range of 2–300 K. The solid curves represent the Curie-Weiss fit results; Figure S15. Field-dependence of the magnetization for **1** (up) and **2** (bottom) in the range of 2–10 K at 0–5 T. The solid curves represent the calculated Brillouin values for non-interacting S_{Gd} spins at 2 K; Figure S16. Field-dependence of the magnetization for **1** (Gd₇) in the range of 3–10 K. The solid curves represent the calculated Brillouin values for non-interacting S_{Gd} spins in the range of 3–10 K, respectively; Figure S17. Field-dependence of the magnetization for **2** (Gd₁₄) in the range of 3–10 K at 0–5 T. The solid curves represent the calculated Brillouin values for non-interacting S_{Gd} spins in the range of 3–10 K, respectively.

Author Contributions: Conceptualization and formal analysis, L.M.; writing—original draft preparation, L.M.; writing—review and editing, supervision, project administration and funding acquisition, H.-Z.K. and C.-M.L. All authors have read and agreed to the published version of the manuscript.

Funding: This research was funded by the National Natural Science Foundation of China, grant numbers 22271171 and 21971142.

Institutional Review Board Statement: Not applicable.

Informed Consent Statement: Not applicable.

Data Availability Statement: The data supporting the reported results are available from the corresponding author.

Conflicts of Interest: The authors declare no conflict of interest.

References

1. Calvez, G.; Le Natur, F.; Daiguebonne, C.; Bernot, K.; Suffren, Y.; Guillou, O. Lanthanide-based hexa-nuclear complexes and their use as molecular precursors. *Coord. Chem. Rev.* **2017**, *340*, 134–153. [CrossRef]
2. Yang, X.P.; Jones, R.A.; Huang, S.M. Luminescent 4f and d-4f polynuclear complexes and coordination polymers with flexible salen-type ligands. *Coord. Chem. Rev.* **2014**, *273*, 63–75. [CrossRef]
3. Ferrando-Soria, J.; Vallejo, J.; Castellano, M.; Martínez-Lillo, J.; Pardo, E.; Cano, J.; Castro, I.; Lloret, F.; Ruiz-García, R.; Julve, M. Molecular magnetism, *quo vadis?* A historical perspective from a coordination chemist viewpoint. *Coord. Chem. Rev.* **2017**, *339*, 17–103. [CrossRef]

4. Georgopoulou, A.N.; Pissas, M.; Psycharis, V.; Sanakis, Y.; Raptopoulou, C.P. Trinuclear NiII-LnIII-NiII Complexes with Schiff Base Ligands: Synthesis, Structure, and Magnetic Properties. *Molecules* **2020**, *25*, 2280. [[CrossRef](#)] [[PubMed](#)]
5. Sheikh, J.A.; Jena, H.S.; Konar, S. Co₃Gd₄ Cage as Magnetic Refrigerant and Co₃Dy₄ Cage Showing Slow Relaxation of Magnetisation. *Molecules* **2022**, *27*, 1130. [[CrossRef](#)] [[PubMed](#)]
6. Chen, W.-P.; Liao, P.-Q.; Yu, Y.; Zheng, Z.; Chen, X.-M.; Zheng, Y.-Z. A mixed-ligand approach for a gigantic and hollow heterometallic cage {Ni₆₄RE₉₆} for gas separation and magnetic cooling applications. *Angew. Chem. Int. Ed.* **2016**, *55*, 9375–9379. [[CrossRef](#)]
7. Li, N.F.; Luo, X.M.; Wang, J.; Wang, J.L.; Mei, H.; Song, Y.; Xu, Y. Largest 3d-4f 196-nuclear Gd₁₅₈Co₃₈ clusters with excellent magnetic cooling. *Sci. China Chem.* **2022**, *65*, 1577–1583. [[CrossRef](#)]
8. Miao, L.; Liu, M.J.; Zeng, M.; Kou, H.Z. Chiral Zn₃Ln₃ Hexanuclear Clusters of an Achiral Flexible Ligand. *Inorg. Chem.* **2023**, *62*, 12814–12821. [[CrossRef](#)]
9. Zeng, M.; Hu, K.Q.; Liu, C.M.; Kou, H.Z. Heterotrimetallic Ni₂Ln₂Fe₃ chain complexes based on [Fe(1-CH₃im)(CN)₅]²⁻. *Dalton Trans.* **2021**, *50*, 6427–6431. [[CrossRef](#)]
10. Jin, Y.S.; Wang, X.; Zhang, N.; Liu, C.M.; Kou, H.Z. Assembly of Hydrazine-Bridged Cyclic Fe^{III}₄Ln^{III}₄ Octanuclear Complexes. *Cryst. Growth Des.* **2022**, *22*, 1263–1269. [[CrossRef](#)]
11. Tian, H.Q.; Bao, S.S.; Zheng, L.M. Cyclic Single-Molecule Magnets: From Even-Numbered Hexanuclear to Odd-Numbered Heptanuclear Dysprosium Clusters. *Eur. J. Inorg. Chem.* **2016**, *19*, 3184–3190. [[CrossRef](#)]
12. Tian, H.Q.; Bao, S.S.; Zheng, L.M. Cyclic single-molecule magnets: From the odd-numbered heptanuclear to a dimer of heptanuclear dysprosium clusters. *Chem. Commun.* **2016**, *52*, 2314–2317. [[CrossRef](#)]
13. Goura, J.; Walsh, J.P.S.; Tuna, F.; Chandrasekhar, V. Synthesis, structure, and magnetism of non-planar heptanuclear lanthanide(III) complexes. *Dalton Trans.* **2015**, *44*, 1142–1149. [[CrossRef](#)] [[PubMed](#)]
14. Mazarakioti, E.C.; Cunha-Silva, L.; Bekiari, V.; Escuer, A.; Stamatatos, T.C. New structural topologies in 4f-metal cluster chemistry from vertex-sharing butterfly units: {Ln^{III}₇} complexes exhibiting slow magnetization relaxation and ligand-centred emissions. *RSC Adv.* **2015**, *5*, 92526–92530. [[CrossRef](#)]
15. Pantelis, K.N.; Perlepe, P.S.; Grammatikopoulos, S.; Lampropoulos, C.; Tang, J.K.; Stamatatos, T.C. 4f-Metal Clusters Exhibiting Slow Relaxation of Magnetization: A {Dy₇} Complex with An Hourglass-like Metal Topology. *Molecules* **2020**, *25*, 2191. [[CrossRef](#)]
16. Peng, J.M.; Wang, H.L.; Zhu, Z.H.; Bai, J.; Liang, F.P.; Zou, H.H. Series of the Largest Dish-Shaped Dysprosium Nanoclusters Formed by in situ Reactions. *Inorg. Chem.* **2022**, *61*, 6094–6100. [[CrossRef](#)]
17. Lu, T.Q.; Yin, J.J.; Chen, C.; Shi, H.Y.; Zheng, J.; Liu, Z.J.; Fang, X.L.; Zheng, X.Y. Two pairs of chiral lanthanide-oxo clusters Ln₁₄ induced by amino acid derivatives. *CrystEngComm* **2021**, *23*, 6923–6929. [[CrossRef](#)]
18. Zhu, Z.H.; Peng, J.M.; Wang, H.L.; Zou, H.H.; Liang, F.P. Assembly Mechanism and Heavy Metal Ion Sensing of Cage-Shaped Lanthanide Nanoclusters. *Cell Rep. Phys. Sci.* **2020**, *1*, 100165. [[CrossRef](#)]
19. Zhang, M.-B.; Zhang, J.; Zheng, S.-T.; Yang, G.-Y. A 3D Coordination Framework Based on Linkages of Nanosized Hydroxo Lanthanide Clusters and Copper Centers by Isonicotinate Ligands. *Angew. Chem. Int. Ed.* **2005**, *44*, 1385–1388. [[CrossRef](#)]
20. Chesman, A.S.R.; Turner, D.R.; Moubaraki, B.; Murray, K.S.; Deacon, G.B.; Batten, S.R. Tetradecanuclear polycarbonatolanthanoid clusters: Diverse coordination modes of carbonate providing access to novel core geometries. *Dalton Trans.* **2012**, *41*, 10903–10909. [[CrossRef](#)]
21. Sun, P.-F.; Zhang, X.-N.; Fan, C.-H.; Chen, W.-P.; Zheng, Y.-Z. Tricine-supported polyoxo(alkoxo)lanthanide cluster {Ln₁₅} (Ln = Eu, Gd, Tb) with magnetic refrigerant and fluorescent properties. *Polyoxometalates* **2023**, *2*, 9140026. [[CrossRef](#)]
22. Du, M.H.; Chen, L.Q.; Jiang, L.P.; Liu, W.D.; Long, L.S.; Zheng, L.S.; Kong, X.J. Counterintuitive Lanthanide Hydrolysis-Induced Assembly Mechanism. *J. Am. Chem. Soc.* **2022**, *144*, 5653–5660. [[CrossRef](#)] [[PubMed](#)]
23. Wang, Q.; Yu, Y.T.; Wang, J.L.; Li, J.N.; Li, N.F.; Fan, X.R.; Xu, Y. Two Windmill-Shaped Ln₁₈ Nanoclusters Exhibiting High Magnetocaloric Effect and Luminescence. *Inorg. Chem.* **2023**, *62*, 3162–3169. [[CrossRef](#)] [[PubMed](#)]
24. Wang, Q.; Lu, S.H.; Xu, L.X.; Wang, J.L.; Yu, Y.T.; Bai, X.; Mei, H.; Xu, Y. C₂O₄²⁻-templated cage-shaped Ln₂₈ (Ln = Gd, Eu) nanoclusters with magnetocaloric effect and luminescence. *Inorg. Chem. Front.* **2023**, *10*, 4109–4116. [[CrossRef](#)]
25. Li, Y.L.; Wang, H.L.; Zhu, Z.H.; Liang, F.P.; Zou, H.H. Giant Crown-Shaped Dy₃₄ Nanocluster with High Acid–Base Stability Assembled by an out-to-in Growth Mechanism. *Inorg. Chem.* **2022**, *61*, 10101–10107. [[CrossRef](#)]
26. Wu, M.; Jiang, F.; Kong, X.; Yuan, D.; Long, L.; Al-Thabaiti, S.A.; Hong, M. Two polymeric 36-metal pure lanthanide nanosize clusters. *Chem. Sci.* **2013**, *4*, 3104–3108. [[CrossRef](#)]
27. Zhou, Y.; Zheng, X.Y.; Cai, J.; Hong, Z.F.; Yan, Z.H.; Kong, X.J.; Ren, Y.P.; Long, L.S.; Zheng, L.S. Three Giant Lanthanide Clusters Ln₃₇ (Ln = Gd, Tb, and Eu) Featuring A Double-Cage Structure. *Inorg. Chem.* **2017**, *56*, 2037–2041. [[CrossRef](#)]
28. Guo, F.S.; Chen, Y.C.; Mao, L.L.; Lin, W.Q.; Leng, J.D.; Tarasenko, R.; Orendac, M.; Prokleska, J.; Sechovsky, V.; Tong, M.L. Anion-Templated Assembly and Magnetocaloric Properties of a Nanoscale {Gd₃₈} Cage versus a {Gd₄₈} Barrel. *Chem.—Eur. J.* **2013**, *19*, 14876–14885. [[CrossRef](#)]
29. Luo, X.M.; Hu, Z.B.; Lin, Q.F.; Cheng, W.; Cao, J.P.; Cui, C.H.; Mei, H.; Song, Y.; Xu, Y. Exploring the Performance Improvement of Magnetocaloric Effect Based Gd-Exclusive Cluster Gd₆₀. *J. Am. Chem. Soc.* **2018**, *140*, 11219–11222. [[CrossRef](#)]
30. Qin, L.; Yu, Y.-Z.; Liao, P.-Q.; Xue, W.; Zheng, Z.; Chen, X.-M.; Zheng, Y.-Z. A “Molecular Water Pipe”: A Giant Tubular Cluster {Dy₇₂} Exhibits Fast Proton Transport and Slow Magnetic Relaxation. *Adv. Mater.* **2016**, *28*, 10772–10779. [[CrossRef](#)]

31. Peng, J.B.; Kong, X.J.; Zhang, Q.C.; Orendac, M.; Prokleska, J.; Ren, Y.P.; Long, L.S.; Zheng, Z.; Zheng, L.S. Beauty, symmetry, and magnetocaloric effect-four-shell keplerates with 104 lanthanide atoms. *J. Am. Chem. Soc.* **2014**, *136*, 17938–17941. [[CrossRef](#)] [[PubMed](#)]
32. Zheng, X.-Y.; Jiang, Y.-H.; Zhuang, G.-L.; Liu, D.-P.; Liao, H.-G.; Kong, X.-J.; Long, L.-S.; Zheng, L.-S. A gigantic molecular wheel of {Gd₁₄₀}: A new member of the molecular wheel family. *J. Am. Chem. Soc.* **2017**, *139*, 18178–18181. [[CrossRef](#)]
33. Wu, Y.-L.; Li, X.-X.; Qi, Y.-J.; Yu, H.; Jin, L.; Zheng, S.-T. {Nb₂₈₈O₇₆₈(OH)₄₈(CO₃)₁₂}: A macromolecular polyoxometalate with close to 300 niobium atoms. *Angew. Chem. Int. Ed.* **2018**, *57*, 8572–8576. [[CrossRef](#)] [[PubMed](#)]
34. Liu, C.-M.; Sun, R.; Hao, X.; Wang, B.-W. Two Pairs of Homochiral Parallelogram-like Dy₄ Cluster Complexes with Strong Magneto-Optical Properties. *Inorg. Chem.* **2023**, *62*, 20184–20193. [[CrossRef](#)]
35. Hao, J.; Geng, L.; Zheng, J.Y.; Wei, J.H.; Zhang, L.L.; Feng, R.; Zhao, J.X.; Li, Q.W.; Pang, J.D.; Bu, X.H. Ligand Induced Double-Chair Conformation Ln₁₂ Nanoclusters Showing Multifunctional Magnetic and Proton Conductive Properties. *Inorg. Chem.* **2022**, *61*, 3690–3696. [[CrossRef](#)] [[PubMed](#)]
36. Gschneidner, K.A.; Pecharsky, V.K. Thirty years of near room temperature magnetic cooling: Where we are today and future prospects. *Int. J. Refrig.* **2008**, *31*, 945–961. [[CrossRef](#)]
37. Evangelisti, M.; Brechin, E.K. Recipes for enhanced molecular cooling. *Dalton Trans.* **2010**, *39*, 4672–4676. [[CrossRef](#)]
38. Koskelo, E.C.; Liu, C.; Mukherjee, P.; Kelly, N.D.; Dutton, S.E. Free-Spin Dominated Magnetocaloric Effect in Dense Gd₃₊ Double Perovskites. *Chem. Mater.* **2022**, *34*, 3440–3450. [[CrossRef](#)]
39. Lorusso, G.; Sharples, J.W.; Palacios, E.; Roubeau, O.; Brechin, E.K.; Sessoli, R.; Rossin, A.; Tuna, F.; McInnes, E.J.L.; Collison, D.; et al. A Dense Metal-Organic Framework for Enhanced Magnetic Refrigeration. *Adv. Mater.* **2013**, *25*, 4653–4656. [[CrossRef](#)]
40. Yang, Y.; Zhang, Q.-C.; Pan, Y.-Y.; Long, L.-S.; Zheng, L.-S. Magnetocaloric effect and thermal conductivity of Gd(OH)₃ and Gd₂O(OH)₄(H₂O)₂. *Chem. Commun.* **2015**, *51*, 7317–7320. [[CrossRef](#)]
41. Palacios, E.; Rodríguez-Velamazán, J.A.; Evangelisti, M.; McIntyre, G.J.; Lorusso, G.; Visser, D.; de Jongh, L.J.; Boatner, L.A. Magnetic structure and magnetocalorics of GdPO₄. *Phys. Rev. B Condens. Matter Mater. Phys.* **2014**, *90*, 214423. [[CrossRef](#)]
42. Chen, Y.-C.; Qin, L.; Meng, Z.-S.; Yang, D.-F.; Wu, C.; Fu, Z.; Zheng, Y.-Z.; Liu, J.-L.; Tarasenko, R.; Orendáč, M.; et al. Study of a magnetic-cooling material Gd(OH)CO₃. *J. Mater. Chem. A* **2014**, *2*, 9851–9858. [[CrossRef](#)]
43. Chen, Y.-C.; Prokleska, J.; Xu, W.-J.; Liu, J.-L.; Liu, J.; Zhang, W.-X.; Jia, J.-H.; Sechovský, V.; Tong, M.-L. A brilliant cryogenic magnetic coolant: Magnetic and magnetocaloric study of ferromagnetically coupled GdF₃. *J. Mater. Chem. C* **2015**, *3*, 12206–12211. [[CrossRef](#)]
44. Xu, Q.F.; Liu, B.L.; Ye, M.Y.; Zhuang, G.L.; Long, L.S.; Zheng, L.S. Gd(OH)F₂: A Promising Cryogenic Magnetic Refrigerant. *J. Am. Chem. Soc.* **2022**, *144*, 13787–13793. [[CrossRef](#)]
45. Chen, Y.W.; Gong, P.F.; Guo, R.X.; Fan, F.D.; Shen, J.; Zhang, G.C.; Tu, H. Improvement on Magnetocaloric Effect through Structural Evolution in Gadolinium Borate Halides Ba₂Gd(BO₃)₂X (X = F, Cl). *Inorg. Chem.* **2023**, *62*, 15584–15592. [[CrossRef](#)] [[PubMed](#)]
46. Liu, M.-J.; Yuan, J.; Tao, J.; Zhang, Y.-Q.; Liu, C.-M.; Kou, H.-Z. Rhodamine Salicylaldehyde Hydrazone Dy(III) Complexes: Fluorescence and Magnetism. *Inorg. Chem.* **2018**, *57*, 4061–4069. [[CrossRef](#)] [[PubMed](#)]
47. Liu, M.-J.; Wu, S.-Q.; Li, J.-X.; Zhang, Y.-Q.; Sato, O.; Kou, H.-Z. Structural Modulation of Fluorescent Rhodamine-Based Dysprosium(III) Single-Molecule Magnets. *Inorg. Chem.* **2020**, *59*, 2308–2315. [[CrossRef](#)] [[PubMed](#)]
48. Liu, M.-J.; Fu, Z.-Y.; Sun, R.; Yuan, J.; Liu, C.-M.; Zou, B.; Wang, B.-W.; Kou, H.-Z. Mechanochromic and Single-Molecule Magnetic Properties of a Rhodamine 6G Dy(III) Complex. *ACS Appl. Electron. Mater.* **2021**, *3*, 1368–1374. [[CrossRef](#)]
49. Miao, L.; Liu, M.J.; Ding, M.M.; Zhang, Y.Q.; Kou, H.Z. A Dy(III) Fluorescent Single-Molecule Magnet Based on a Rhodamine 6G Ligand. *Inorganics* **2021**, *9*, 51. [[CrossRef](#)]
50. Yuan, J.; Wu, S.Q.; Liu, M.J.; Sato, O.; Kou, H.Z. Rhodamine 6G-Labeled Pyridyl Aroylhydrazone Fe(II) Complex Exhibiting Synergetic Spin Crossover and Fluorescence. *J. Am. Chem. Soc.* **2018**, *140*, 9426–9433. [[CrossRef](#)]
51. Yuan, J.; Liu, M.-J.; Wu, S.-Q.; Zhu, X.; Zhang, N.; Sato, O.; Kou, H.-Z. Substituent effects on the fluorescent spin-crossover Fe(ii) complexes of rhodamine 6G hydrazones. *Inorg. Chem. Front.* **2019**, *6*, 1170–1176. [[CrossRef](#)]
52. Huang, W.; Wu, D.; Guo, D.; Zhu, X.; He, C.; Meng, Q.; Duan, C. Efficient near-infrared emission of a Ytterbium(III) compound with a green light rhodamine donor. *Dalton Trans.* **2009**, *12*, 2081–2084. [[CrossRef](#)] [[PubMed](#)]
53. Sharples, J.W.; Zheng, Y.Z.; Tuna, F.; McInnes, E.J.L.; Collison, D. Lanthanide discs chill well and relax slowly. *Chem. Commun.* **2011**, *47*, 7650–7652. [[CrossRef](#)] [[PubMed](#)]
54. Xu, C.Y.; Wu, Z.L.; Fan, C.J.; Yan, L.L.; Wang, W.M.; Ji, B.M. Synthesis of two lanthanide clusters Ln^{III}₄ (Gd₄ and Dy₄) with [2 × 2] square grid shape: Magnetocaloric effect and slow magnetic relaxation behaviors. *J. Rare Earths* **2021**, *39*, 1082–1088. [[CrossRef](#)]
55. Wang, W.M.; Li, X.Z.; Zhang, L.; Chen, J.L.; Wang, J.H.; Wu, Z.L.; Cui, J.Z. A series of [2 × 2] square grid Ln^{III}₄ clusters: A large magnetocaloric effect and single-molecule-magnet behavior. *New J. Chem.* **2019**, *43*, 7419–7426. [[CrossRef](#)]
56. Baril-Robert, F.; Petit, S.; Pilet, G.; Chastanet, G.; Reber, C.; Luneau, D. Site-Selective Lanthanide Doping in a Nonanuclear Yttrium(III) Cluster Revealed by Crystal Structures and Luminescence Spectra. *Inorg. Chem.* **2010**, *49*, 10970–10976. [[CrossRef](#)]
57. Petit, S.; Baril-Robert, F.; Pilet, G.; Reber, C.; Luneau, D. Luminescence spectroscopy of europium(III) and terbium(III) penta-, octa- and nonanuclear clusters with β-diketonate ligands. *Dalton Trans.* **2009**, *34*, 6809–6815. [[CrossRef](#)]
58. Wang, R.; Song, D.; Wang, S. Toward constructing nanoscale hydroxo-lanthanide clusters: Syntheses and characterizations of novel tetradecanuclear hydroxo-lanthanide clusters. *Chem. Commun.* **2002**, *4*, 368–369. [[CrossRef](#)]

59. Li, X.-L.; He, L.-F.; Feng, X.-L.; Song, Y.; Hu, M.; Han, L.-F.; Zheng, X.-J.; Zhang, Z.-H.; Fang, S.-M. Two chiral tetradecanuclear hydroxo-lanthanide clusters with luminescent and magnetic properties. *CrystEngComm* **2011**, *13*, 3643–3645. [[CrossRef](#)]
60. Bürgstein, M.R.; Gamer, M.T.; Roesky, P.W. Nitrophenolate as a building block for lanthanide chains, layers, and clusters. *J. Am. Chem. Soc.* **2004**, *126*, 5213–5218. [[CrossRef](#)]

Disclaimer/Publisher’s Note: The statements, opinions and data contained in all publications are solely those of the individual author(s) and contributor(s) and not of MDPI and/or the editor(s). MDPI and/or the editor(s) disclaim responsibility for any injury to people or property resulting from any ideas, methods, instructions or products referred to in the content.